Chinese Chemical Letters 36 (2025) 110280

Contents lists available at ScienceDirect

Chinese Chemical Letters

journal homepage: www.elsevier.com/locate/cclet

Discovery of an activatable near-infrared fluorescent and theranostic PROTAC for tumor-targeted detecting and degrading of BRD4

Keliang Li, Guoqiang Dong, Shanchao Wu*, Chunquan Sheng*

The Center for Basic Research and Innovation of Medicine and Pharmacy (MOE), School of Pharmacy, Second Military Medical University (Naval Medical University), Shanghai 200433, China

ARTICLE INFO

Article history:
Received 7 May 2024
Revised 12 July 2024
Accepted 17 July 2024
Available online 18 July 2024

Keywords:
PROTAC
Near-infrared
Theranostic
BRD4
Tumor-targeted

ABSTRACT

Proteolysis-targeting chimera (PROTAC) has emerged as an efficient strategy to accurately control intracellular protein levels. However, conventional PROTACs are generally limited by nonspecific protein degradation and off-tissue side effects. Particularly, there is a lack of effective chemical tools for visualizing protein degradation. Herein, a near-infrared fluorescent and theranostic PROTAC (**PRO-S-DCM**) was designed for imaging the degradation of bromodomain-containing protein 4 (BRD4). **PRO-S-DCM** could be tumor-specifically activated and exhibited favorable imaging effects both *in vitro* and *in vivo*. **PRO-S-DCM** was proven to be a theranostic probe, which potently inhibited growth, invasion and migration of HeLa cells and induced cell apoptosis.

Proteolysis-targeting chimera (PROTAC) is emerging as a promising technology to control intracellular protein levels and has attracted considerable interests in drug discovery and development [1,2]. Specifically, PROTACs hijack the endogenous E3 ubiquitin ligase to protein of interest (POI) by forming ternary complex and trigger protein degradation by the ubiquitin-proteasome system (UPS) [3,4]. Compared with traditional occupancy-driven inhibitors, the event-driven mechanism of PROTACs possess distinct advantages, including catalytic nature, longer-lasting effects and expanded target space [5,6]. To date, a large number of PROTACs have been designed to degrade hundreds of drug targets and more than twenty PROTACs are currently evaluated in clinical trials [7-10].

Despite the unique features of PROTACs, there are also several major limitations of conventional PROTAC molecules, such as large molecular weight, unfavorable pharmacokinetic properties, nonspecific protein degradation and off-tissue side effects [11]. In particular, systemic administration of PROTACs would cause unwanted accumulation at off-target sites, leading to undesired toxicity [12]. Nevertheless, precise target protein degradation still remains a major challenge. Therefore, there is urgent need to develop new strategies for real-time detecting and tracking the protein degradation. Previously, our group designed the first fluorescent PROTAC, enabling the visualization of protein degradation in living cells [13]. However, the PROTAC probe was designed from a fluorescent ligand with the maximum emission wavelength (λ_{em}) of 450 nm, which is restricted by poor tissue penetration.

Near-infrared (NIR) probes have the advantages of low invasiveness, deep tissue penetration and reduced toxicity, which were developed as indispensable tools in chemical biology and precise medicine [14,15]. However, direct introduction of NIR fluorophores on PROTACs may block the protein degrading activity. Taking the advantages of stimuli-activatable PROTACs developed by our group and others [16-18], we envisioned that attaching NIR fluorophore to the PROTAC through an activatable linker could simultaneously realize imaging, targeting and protein-degrading effects.

Bromodomain-containing protein 4 (BRD4) belongs to the bromodomain and extraterminal (BET) protein family with tandem bromodomains (BDs) that interact with hyper-acetylated histone regions along the chromatin, accumulating on transcriptionally active regulatory elements to promote gene transcription at initiation and elongation phases [19]. Upregulated expression of BRD4 is closely related to the development of multiple tumors, which has been considered as a promising antitumor drug target [20,21]. Currently, a large number of PROTACs have been designed to degrade BRD4 (Fig. 1) [8]. However, off-tissue side effects of BRD4 PROTAC ARV-771 were also reported [22].

Herein, we designed an NIR PROTAC probe (**PRO-S-DCM**, Scheme S1 in Supporting information) for detection and degradation of BRD4. **PRO-S-DCM** could be selectively activated by endogenous glutathione (GSH) in tumor cells and exerted dual functions of fluorescence imaging and BRD4 degradation (Fig. 2A).

* Corresponding authors.
E-mail addresses: wushanchao07_2@126.com (S. Wu), shengcq@smmu.edu.cn (C. Sheng).

https://doi.org/10.1016/j.cclet.2024.110280
1001-8417/

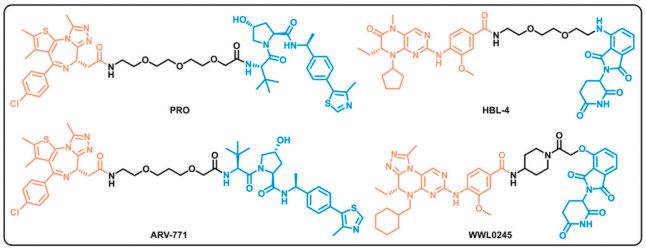

Fig. 1. Representative BRD4 PROTACs.

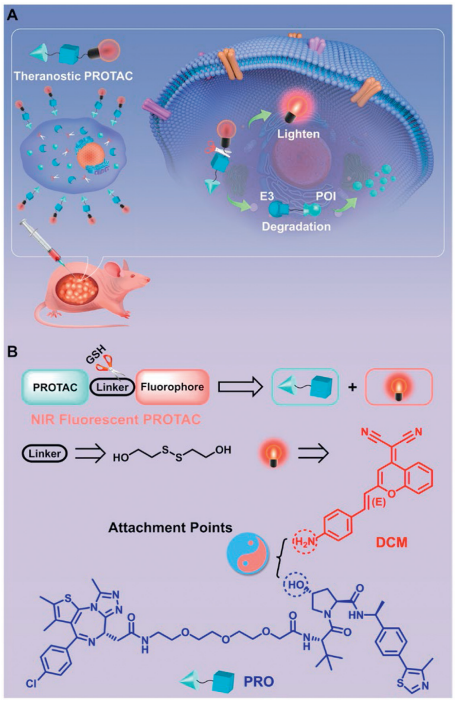

Fig. 2. Design of NIR fluorescent and theranostic PROTAC probe. (A) Schematic diagram of the design strategy of PROTAC-based theranostic probe. NIR fluorophore and PROTAC are connected through an activable linker. The cleavable linker is attacked by GSH to release the original PROTAC for degradation and fluorophore for imaging. (B) Design rationale of NIR fluorescent PROTAC **PRO-S-DCM**.

PRO-S-DCM was also a theranostic probe, which showed potent antitumor activity against HeLa cells.

Previous studies indicated that the alkylation of the hydroxyl group in the von Hippel-Lindau (VHL) ligand would eliminate the protein degradation activity [1,23]. Therefore, an NIR fluorescent PROTAC was rationally designed by introducing NIR fluorophore onto the VHL hydroxyl group of BRD4 PROTAC through an activable linker. Considering that tumor cells have higher endogenous glutathione (GSH) content than normal cells [24], disulfide bond that could be selectively recognized by GSH was selected as the cleavable site. Dicyanomethylene-4*H*-pyran derivative **DCM** was used as the NIR fluorescent group because it possessed maximum emission wavelength (λ_{em}) in the NIR region (650–900 nm), large Stokes shift and high photostability [25]. The potent BRD4 degrader **PRO** was selected as the original PROTAC, as **PRO** has been widely employed as a template molecule for PROTAC-based proof of concept [18]. As a result, NIR fluorescent PROTAC **PRO-S-DCM** was rationally designed, which was expected to be activated by nucleophilic attack of abundant endogenous GSH and then release **PRO** and **DCM**, respectively (Fig. 2B). Negative control **PRO-C-DCM** with an uncleavable alkane linker was also designed.

The synthetic route for preparation of NIR fluorescent PROTAC is shown in Scheme S1. 2-(2-Methyl-4*H*-chromen-4-ylidene)malononitrile (**1**) was treated with *N*-(4-formylphenyl)acetamide (**2**) to afford fluorophore **DCM** *via* Knoevenagel and deacetylation reactions at high temperatures. VHL ligand **4** was acylated with 4-nitrophenyl carbonochloridate in the presence of 4-(dimethylamino)pyridine (DMAP) to give intermediate **6**, which was further reacted with 2,2′-disulfanediylbis(ethan-1-ol) to afford intermediate **7**. Then, intermediate **9** was prepared by the deprotection of intermediate **7** in the presence of trifluoroacetic acid (TFA), followed by a condensation reaction with the polyethylene glycol linker. Compound **10** was obtained by the deprotection of intermediate **9**, which was further condensed with commercially available (+)-**JQ1** carboxylic acid in the presence of 1-[bis(dimethylamino)methylene]−1*H*-1,2,3-triazolo[4,5-*b*]pyridinium 3-oxide hexafluorophosphate (HATU) and *N*,*N*-diisopropylethylamine (DIPEA) to afford key intermediate **PRO-S**. Finally, target compound **PRO-S-DCM** was obtained by forming a carbonate bond between **DCM** and **PRO-S** in the presence of triphosgene. Synthesis of negative control **PRO-C-DCM** and BRD4 degrader **PRO** were depicted in Schemes S2 and S3 (Supporting information).

Initially, the release of **PRO-S-DCM** in the presence of GSH was verified by high performance liquid chromatography (HPLC). Without exogenous GSH, **PRO-S-DCM** remained stable (Fig. S1A in Supporting information). In contrast, under the activation of excessive GSH (10 mmol/L) within 6 h, **PRO-S-DCM** (1 mmol/L) was completely transformed into BRD4 PROTAC **PRO** (retention time (RT) = 18.55 min) and NIR fluorophore **DCM** (RT = 23.55 min), respectively. The activation of **PRO-S-DCM** by GSH was also confirmed by liquid chromatograph-mass spectrometer (LC-MS) with the same gradient elution conditions (Fig. S1B in Supporting information). To further validate *in vitro* drug release, the spectral properties of target compounds in dimethyl sulfoxide (DMSO) were further tested (Table S1 and Fig. S2 in Supporting information). The maximum emission wavelengths of **PRO-S-DCM** (λ_{em} = 557 nm) and **PRO-C-DCM** (λ_{em} = 560 nm) were significantly shorter than that of the fluorophore **DCM** (λ_{em} = 647 nm). However, upon the addition of GSH (10 mmol/L), the fluorescence spectral of **PRO-S-DCM** (1 mmol/L) was changed with a new maximum emission wavelength appearing at 647 nm in DMSO, which was the same as that of **DCM** (Figs. 3A and B). On the contrary, the spectral prop-

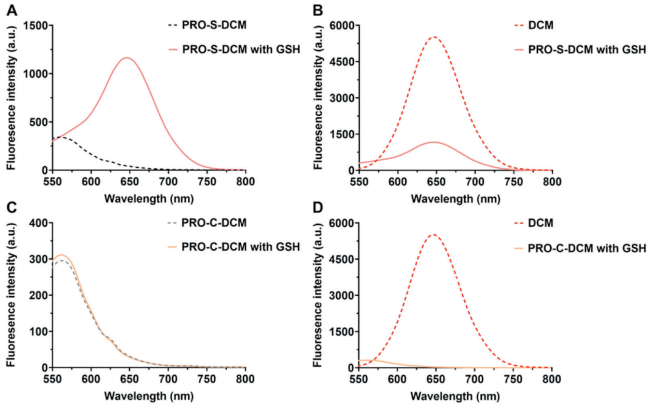

Fig. 3. The changes of the emission spectrum of probe **PRO-S-DCM** and negative control **PRO-S-DCM** in the presence of GSH. (A) Comparison of the emission spectra of **PRO-S-DCM** (1 mmol/L) in DMSO with and without GSH (10 mmol/L). (B) Comparison of the emission spectra of **PRO-S-DCM** (1 mmol/L) with GSH (10 mmol/L) and **DCM** (1 mmol/L) in DMSO. (C) Comparison of the emission spectra of **PRO-C-DCM** (1 mmol/L) in DMSO with and without GSH (10 mmol/L). (D) Comparison of the emission spectra of **PRO-C-DCM** (1 mmol/L) with GSH (10 mmol/L) and **DCM** (1 mmol/L) in DMSO.

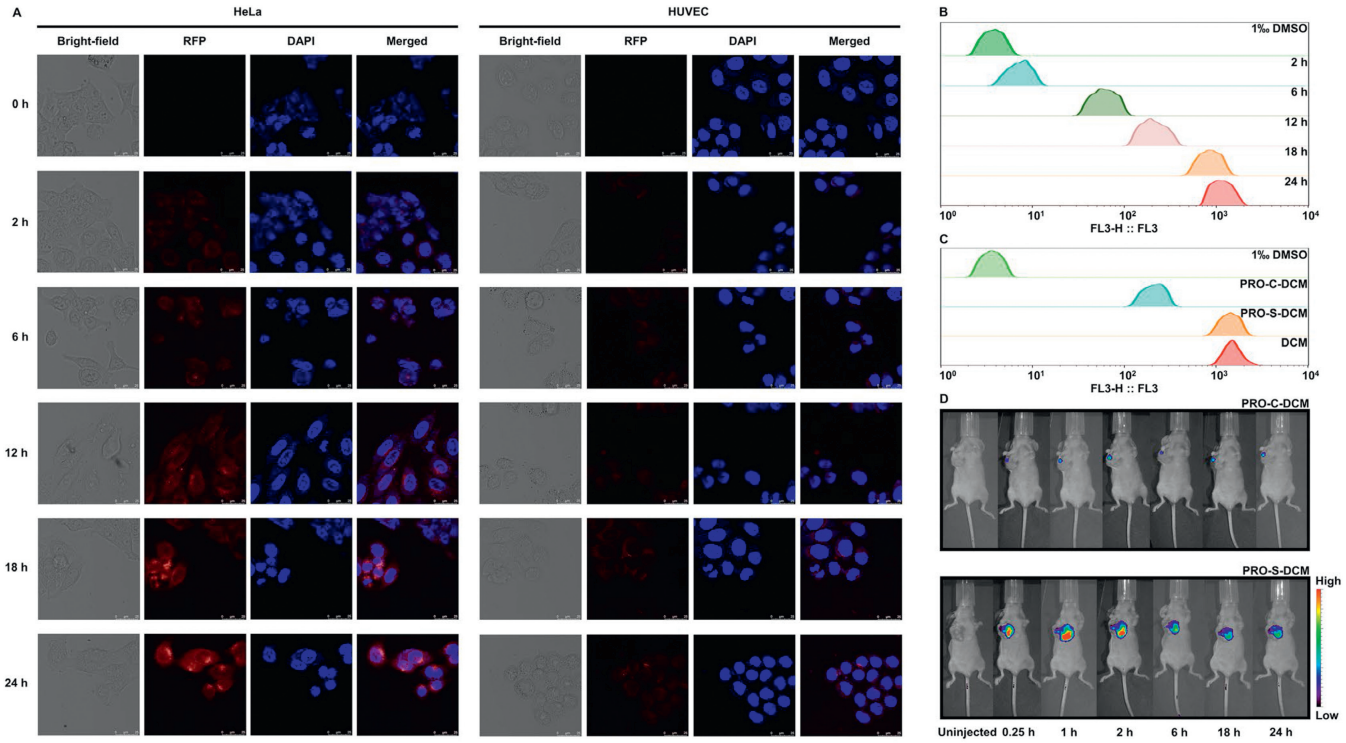

Fig. 4. *In vitro* and *in vivo* imaging effects of target compounds. (A) The time-dependent confocal fluorescence imaging of **PRO-S-DCM** in HeLa and HUVEC cells (10 μmol/L). Scale bar: 25 μm. (B) The time-dependent flow cytometry results of HeLa cells staining by **PRO-S-DCM** (10 μmol/L). (C) The flow cytometry results of **PRO-C-DM**, **PRO-S-DCM** and **DCM** incubated with HeLa cells (10 μmol/L) for 24 h. (D) Imaging effects of **PRO-C-DCM** and **PRO-S-DCM** on xenograft tumor-bearing nude mice after intratumor injection (5 mg/kg, excitation wavelength = 500 nm, detection wavelength = 660 nm). RFP: red fluorescent protein; DAPI: 4′,6-diamidino-2-phenylindole.

erties of negative control **PRO-C-DCM** were unchanged upon the treatment with GSH (Figs. 3C and D). Furthermore, the activation of **PRO-S-DCM** was not interfered by other substances besides GSH (Fig. S3 in Supporting information). The results demonstrated that **PRO-S-DCM** could be specifically activated by GSH to release BRD4 PROTAC **PRO** and NIR fluorophore **DCM** *in vitro*.

Prior to the evaluation of the imaging effects and antitumor activity of **PRO-S-DCM**, cervical cancer cell line (HeLa) with high expression of BRD4 and human umbilical vein endothelial cell line (HUVEC) were selected to measure the endogenous GSH content. The results indicated that GSH content in HeLa cells (358.50 μmol/gprot) was significantly higher than that in normal cells (100.98 μmol/gprot, Fig. S4 in Supporting information).

Based on the verified drug release of **PRO-S-DCM** and definite endogenous GSH content, time-dependent confocal fluorescence imaging was performed on HeLa and HUVEC cells to evaluate staining effects of **PRO-S-DCM** (Fig. 4A). After the addition of **PRO-S-DCM** (10 μmol/L), faint red fluorescence was observed in HeLa cells at 2 h. With the extension of incubation time, the fluorescence intensity was increased gradually with a maximum fluorescence intensity at 24 h. In contrast, the fluorescence intensity of HUVEC cells was significantly weaker than that of HeLa cells at each time point. The staining effects of **PRO-S-DCM** were further quantitatively analyzed by flow cytometry analysis. As shown in Fig. 4B, HeLa cells exhibited a gradual fluorescence intensity increase with prolonged incubation time and the maximum effect was observed at 24 h. In addition, the labeling effects of **DCM**, **PRO-S-DCM** and **PRO-C-DCM** were also verified by flow cytometry analysis. As expected, the labeling effect of **PRO-S-DCM** on HeLa cells was comparable to that of NIR fluorophore **DCM** (Fig. 4C). However, the fluorescence intensity of **PRO-C-DCM**-labeled cells was much weaker than that of **PRO-S-DCM**. These results demonstrated that **PRO-S-DCM** could be used as an effective tool for selective labeling of tumor cells based on the differences in endogenous GSH levels, which prompted us to further investigate the *in vivo* imaging of xenograft tumor nude mice.

Before the animal studies, the *in vitro* metabolic stability of **PRO-S-DCM** was evaluated using the Institute of Cancer Research (ICR) mouse liver microsome assay (Table S2 and Fig. S5 in Supporting information). **PRO-S-DCM** exhibited proper metabolic properties with a terminal half-life ($t_{1/2}$) of 14.71 min and an intrinsic clearance (CL_{int}) of 94.20 mL min^{-1} kg^{-1}. To determine the *in vivo* fluorescent imaging effects of **PRO-S-DCM**, the HeLa xenograft mouse model was prepared and **PRO-C-DCM** was used as the negative control. The experimental procedures, the animal use and care protocols were approved by the Committee on Ethics of Biomedicine, Navy Medical University. Two compounds were respectively injected into the tumors at a dose of 5 mg/kg, then NIR images were captured at different time points. As shown in Fig. 4D, the fluorescence intensity of **PRO-S-DCM** could be observed within 0.25 h, then reached the maximum fluorescence intensity at 1 h and decreased with time prolonged. In contrast, the negative control showed consistently weaker fluorescence intensity. Furthermore, the tumor and major organs of experimental nude mice were harvested for imaging and the tumor showed the strongest fluorescence intensity, which indicated that **PRO-S-DCM** could be selectively activated by endogenous GSH in tumor tissue (Fig. S6 in Supporting information). These results demonstrated that highly active **PRO-S-DCM** can be rapidly activated by intra-tumoral GSH to release BRD4 PROTAC **PRO** and near-infrared fluorophore **DCM** *in vivo*.

BRD4 degradation effects of **PRO-S-DCM** and **PRO-C-DCM** in HeLa and HUVEC cells were further conducted by Western blot analysis. As shown in Figs. 5A and B and Fig. S7 (Supporting information), BRD4 in HeLa cells could be degraded by **PRO-S-DCM** at the concentration range of 100 nmol/L to

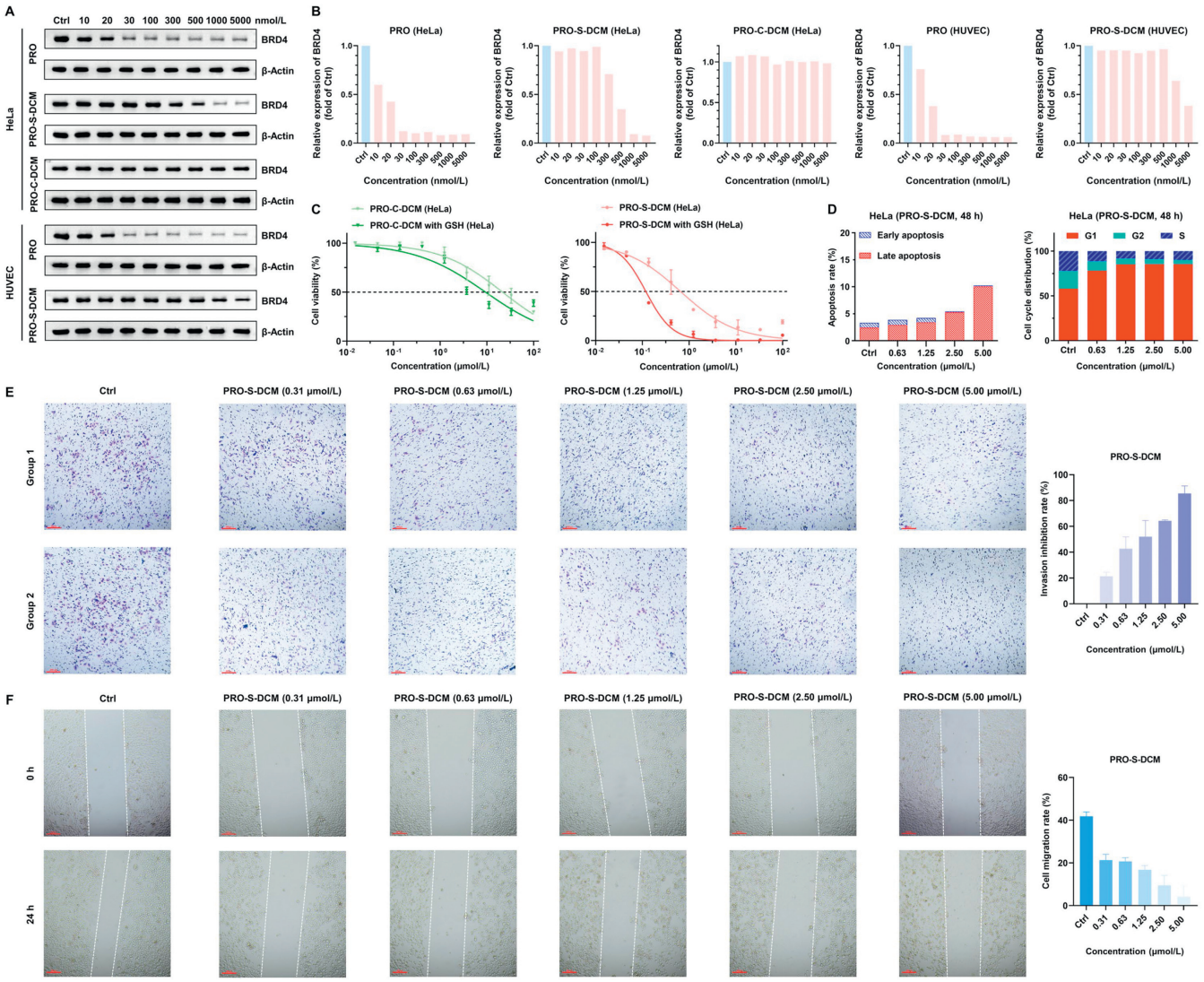

Fig. 5. BRD4 degradation and *in vitro* antitumor activity of target compounds. (A) The BRD4 levels in HeLa and HUVEC cells treated with **PRO**, **PRO-S-DCM** and **PRO-C-DCM** at various concentrations for 24 h. (B) Intensity quantification of the Western blot bands. (C) Cytotoxicity of **PRO-S-DCM** and **PRO-C-DCM** in HeLa cells with and without exogenous GSH (2.50 mmol/L), as determined by a CCK-8 assay. (D) Cell apoptosis and cycle arrest effects of **PRO-S-DCM** in HeLa cells. (E) Inhibition effects of invasion by **PRO-S-DCM** against HeLa cells (two parallel experiments). (F) Inhibition effects of migration by **PRO-S-DCM** against HeLa cells ($n = 3$). The error bars indicate the mean ± standard deviation (SD) values. Scale bar: 200 μm.

5 μmol/L in a dose-dependent manner (half-degradation concentration (DC_{50}) = 408.10 nmol/L, maximum degradation (D_{max}) > 92%), while the degradation activity of **PRO-S-DCM** was decreased about 7-fold in HUVEC (DC_{50} = 2.90 μmol/L). Potentially owing to insufficient drug release in HeLa cells, **PRO-S-DCM** was less active than positive control **PRO** (DC_{50} = 13.10 nmol/L, D_{max} > 91%). However, the BRD4 degradation activity of **PRO-S-DCM** was enhanced upon the addition of 2.50 mmol/L exogenous GSH (DC_{50} = 277.70 nmol/L, Fig. S8 in Supporting information). Even though, **PRO-S-DCM** showed better tumor targeting than **PRO**, because **PRO** remained similar BRD4 degradation in normal HUVEC cells (DC_{50} = 15.70 nmol/L, D_{max} > 93%). Additionally, the negative control **PRO-C-DCM** failed to degrade BRD4. These results verified that **PRO-S-DCM** exhibited effective and tumor-specific BRD4 degradation.

Additionally, the *in vitro* antitumor activity and cytotoxicity of target compounds were further tested using the cell counting kit-8 (CCK-8) assay (Table S3 and Fig. S9 in Supporting information). **PRO-S-DCM** showed potent antitumor activity against HeLa cells (half-inhibitory concentration (IC_{50}) = 0.68 μmol/L). Compared with **PRO-S-DCM**, the negative control **PRO-C-DCM** showed a 32-fold decrease of inhibitory activity against HeLa cells (IC_{50} = 21.72 μmol/L). As shown in Fig. 5C, the antitumor activity of **PRO-S-DCM** was further increased about 6-fold (IC_{50} = 0.12 μmol/L) after the addition of exogenous GSH (2.50 mmol/L), whereas **PRO-C-DCM** still showed weak antitumor activity (IC_{50} = 10.09 μmol/L). Compared with the original PROTAC **PRO** possessing similar antitumor activity and cytotoxicity (HeLa, IC_{50} = 17.67 nmol/L; HUVEC, IC_{50} = 26.52 nmol/L), **PRO-S-DCM** showed significantly reduced cytotoxicity in HUVEC cells (IC_{50} = 4.51 μmol/L), and **PRO-C-DCM** remained inactive (IC_{50} = 31.54 μmol/L). These results further indicated that **PRO-S-DCM** could be activated by GSH to release **PRO** and exert antitumor effects, which were consistent with the results of BRD4 degradation.

Uncontrolled cell growth is one of the primary characteristics of tumor cells [26]. The induction of cell apoptosis and regulation of cell cycle distribution contribute to the growth inhibition of tumor cells. Thus, flow cytometry analysis was performed to explore the influence of **PRO-S-DCM** on the induction of cell apoptosis and cell cycle distribution. As shown in Fig. 5D and Fig. S10 (Supporting

information), after the incubation with **PRO-S-DCM** at the concentrations of 0.63, 1.25, 2.50 and 5.00 μmol/L for 48 h, the number of apoptotic HeLa cells was increased to 3.87%, 4.20%, 5.42% and 10.24%, respectively, while the percentages of apoptotic cells in the control group was only 3.32%. Furthermore, **PRO-S-DCM** could arrest HeLa cell cycles at the G1/M stage in a dose-dependent manner. These results indicated that **PRO-S-DCM** dose-dependently induced apoptosis in HeLa cells and cycle arrest at the G1/M phase.

It is well-acknowledged that tumor metastasis is one of the major causes of tumor-related deaths [26]. Inhibition of tumor cell metastasis reflects the antitumor effects of drugs. We further evaluated the anti-metastasis capacity of **PRO-S-DCM** by cell invasion and migration (transwell and wound-healing) assays. Specifically, the transwell assay manifested that **PRO-S-DCM** dose-dependently decreased the number of HeLa cells invading into the lower compartment and the invasion inhibition rate was larger than 80% at a concentration of 5.00 μmol/L (Fig. 5E), demonstrating that **PRO-S-DCM** efficiently inhibited invasion capacity against HeLa cells. Additionally, wound-healing assays were performed to examine the migration inhibition ability of **PRO-S-DCM** against the HeLa cell line. As depicted in Fig. 5F, the scratched area in the blank control decreased distinctly with the cell migration rate greater than 40%. **PRO-S-DCM** dose-dependently restrained the wound healing and the cell migration rate was reduced to less than 10% at the concentration of 5.00 μmol/L. In contrast, the negative control **PRO-C-DCM** only exhibited weak inhibitory activity against cell invasion and migration (Figs. S11 and S12 in Supporting information).

In summary, based on BRD4 PROTAC **PRO** and fluorophore **DCM**, we developed a novel tumor-targeted activatable NIR theranostic BRD4 PROTAC, possessing both BRD4 degradation activity and fluorescence imaging property. Activated by GSH, **PRO-S-DCM** successfully released original PROTAC for BRD4 degradation and NIR fluorophore for tumor imaging both *in vitro* and *in vivo*. **PRO-S-DCM** was proven to be an NIR fluorescent and theranostic PROTAC probe, which had tumor-specific BRD4 degradation activity and reduced cytotoxicity, induced HeLa cell apoptosis, and inhibited tumor cell metastasis. Taken together, this work highlighted the degradative and imaging potential of tumor-targeted NIR fluorescent theranostic PROTAC and provided a paradigm for expanding the applications of PROTACs in tumor treatment. Moreover, **PRO-S-DCM** provides a new strategy for the improvement of diagnosis and therapeutic of BRD4 PROTACs.

Declaration of competing interest

The authors declare that they have no known competing financial interests or personal relationships that could have appeared to influence the work reported in this paper.

CRediT authorship contribution statement

Keliang Li: Writing – original draft, Validation, Data curation. **Guoqiang Dong:** Supervision, Methodology. **Shanchao Wu:** Writing – review & editing, Funding acquisition, Conceptualization. **Chunquan Sheng:** Writing – review & editing, Funding acquisition, Conceptualization.

Acknowledgments

This work was supported by the National Key Research and Development Program of China (No. 2022YFC3401500 to C. Sheng), the National Natural Science Foundation of China (No. 82030105 to C. Sheng and Nos. 22077138, 22377145 to S. Wu) and Shanghai Rising-Star Program (No. 22QA1411300 to S. Wu).

Supplementary materials

Supplementary material associated with this article can be found, in the online version, at doi:10.1016/j.cclet.2024.110280.

References

[1] A.C. Lai, C.M. Crews, Nat. Rev. Drug Discov. 16 (2017) 101–114.
[2] C. Cao, M. He, L. Wang, Y. He, Y. Rao, Chem. Soc. Rev. 51 (2022) 7066–7114.
[3] G.M. Burslem, C.M. Crews, Cell 181 (2020) 102–114.
[4] C. Pu, S. Wang, L. Liu, et al., Chin. Chem. Lett. 34 (2023) 107927.
[5] M. Schapira, M.F. Calabrese, A.N. Bullock, C.M. Crews, Nat. Rev. Drug Discov. 18 (2019) 949–963.
[6] K. Li, C.M. Crews, Chem. Soc. Rev. 51 (2022) 5214–5236.
[7] A. Mullard, Nat. Rev. Drug Discov. 20 (2021) 247–250.
[8] S. He, G. Dong, J. Cheng, Y. Wu, C. Sheng, Med. Res. Rev. 42 (2022) 1280–1342.
[9] M. He, C. Cao, Z. Ni, et al., Signal Transduct. Target. Ther. 7 (2022) 181.
[10] M. Li, Y. Zhi, B. Liu, Q. Yao, J. Med. Chem. 66 (2023) 2308–2329.
[11] M. Békés, D.R. Langley, C.M. Crews, Nat. Rev. Drug Discov. 21 (2022) 181–200.
[12] K. Moreau, M. Coen, A.X. Zhang, et al., Br. J. Pharmacol. 177 (2020) 1709–1718.
[13] J. Cheng, S. He, J. Xu, et al., J. Med. Chem. 65 (2022) 15725–15737.
[14] H. Li, Y. Kim, H. Jung, J.Y. Hyun, I. Shin, Chem. Soc. Rev. 51 (2022) 8957–9008.
[15] S. He, S. Zhang, X. Zhao, et al., Chin. Chem. Lett. 33 (2022) 4233–4237.
[16] J. Gao, L. Yang, S. Lei, et al., Sci. Bull. 68 (2023) 1069–1085.
[17] Q. He, L. Zhou, D. Yu, et al., J. Med. Chem. 66 (2023) 10458–10472.
[18] S. He, F. Gao, J. Ma, et al., Angew. Chem. Int. Ed. 60 (2021) 23299–23305.
[19] A. Stathis, F. Bertoni, Cancer Discov. 8 (2018) 24–36.
[20] B. Donati, E. Lorenzini, A. Ciarrocchi, Mol. Cancer 17 (2018) 164.
[21] A. Chen, Y. Zhong, Y. Liu, et al., Chin. Chem. Lett. 34 (2023) 107923.
[22] K. Raina, J. Lu, Y. Qian, et al., Proc. Natl. Acad. Sci. U. S. A. 113 (2016) 7124–7129.
[23] J.H. Min, H. Yang, M. Ivan, et al., Science 296 (2002) 1886–1889.
[24] L. Kennedy, J.K. Sandhu, M.E. Harper, M. Cuperlovic-Culf, Biomolecules 10 (2020) 1429.
[25] X. Wu, X. Sun, Z. Guo, et al., J. Am. Chem. Soc. 136 (2014) 3579–3588.
[26] H. Liang, W. Wang, F. Zhu, et al., Bioorg. Med. Chem. 65 (2022) 116793.